Journal of Thermal Analysis and Calorimetry
https://doi.org/10.1007/s10973-023-12437-1

Body temperature NiTi alloys: effect of the heat treatment on the functional thermo-mechanical properties

Davide Ninarello[1] · **Francesca Passaretti**[1] · **Adelaide Nespoli**[1]

Received: 17 February 2023 / Accepted: 23 July 2023

Abstract
The design process of devices based on shape memory alloys (SMA) is particularly demanding. It is fundamental the investigation of parameters describing the thermo-mechanical behavior of these materials, such as the phase transformation temperatures and the Clausius-Clapeyron coefficient (*CCC*). The aim of this study is to determine how heat treatment (HT) affects the above-mentioned parameters on two commercially available body-temperature NiTi alloys. This analysis is accomplished through differential scanning calorimetry (DSC) and strain recovery (SR) tests. Finally, the two NiTi alloys have been compared to determine whether exists a significant difference between different casting batches of the same commercial alloy conformed to the ASTM F2063. It results that both alloys present a similar overall trend of *Af* as a function of HT temperature and time, even if the values significantly differ for treatment at temperatures higher than 773 K for all HT times. Furthermore, it is noted that the HT time presents a minor effect on the value of *Af*. After the SR analysis, it has been possible to highlight the effect of the HT on the values of *CCC* for *As*, *Ms* and *Rs*. The overall trend is similar between the two NiTi alloys. These results lead to the conclusion that HT highly affect not only the transformation temperatures but also the transformation path of the alloy, thus its mechanical properties.

Keywords Shape memory alloy · Body-temperature · NiTi · Characteristic temperatures · Clausius-Clapeyron

Introduction

Ni–Ti alloy, inasmuch shape memory alloy (SMA), presents two principal properties: pseudoelasticity (PE) and shape memory effect (SME) [1]. The former is the ability to recover high strains during unloading in isothermal conditions, while the latter allows to recover a pre-set parental shape by heating the deformed sample above a characteristic temperature of the material. Both properties are allowed thanks to a first-order and reversible thermo-elastic transformation between two solid phases: a B19' monocline Martensite (M), stable at low temperatures, and a B2 body centered cubic Austenite (A), stable at high temperatures. The phase transformation between austenite and martensite (and vice versa) is marked by the passage through characteristic temperatures. These are four: Martensite start temperature (*Ms*), Martensite finish temperature (*Mf*), Austenite start temperature (*As*) and Austenite finish temperature (*Af*). For particular thermo-mechanical conditions, a trigonal phase (R) can appear, identified by the R-phase start temperature (*Rs*) and the R-phase finish temperature (*Rf*). The R-phase is characterized by a trigonal structure which could be seen as a deformation of the austenite crystal structure resulting to be an intermediate phase between A and M [2] and can affect the mechanical behavior of the alloy [3].

The transformation temperatures and so the main thermo-mechanical properties of NiTi are highly dependent on both the Ni–Ti ratio and the thermo-mechanical history of the alloy: heat treatments (HT) are typically used to improve the thermal properties and performance of these alloys. The thermal treatment of Ni-rich NiTi (Ni content higher than 50.5 at.% [4]) determines variations in the chemical composition of the matrix, as a consequence of the formation of precipitates. Several works analyzed the generation of precipitates as a consequence of thermal treatment, such as the milestone works of Nishida et al. [5] on 50.8 at.% Ni- Ti and 51.96 at.% Ni- Ti alloys and of Miyazaki et al. [6] on 49.8, 50.6 and 51.6 at.% Ni–Ti

✉ Davide Ninarello
davide.ninarello@icmate.cnr.it

[1] Consiglio Nazionale delle Ricerche – Istituto di Chimica della Materia Condensata e di Tecnologie per l'Energia (CNR-ICMATE), via G. Previati 1/e, 23900 Lecco, Italy

Published online: 28 August 2023

alloys. These works shed light on the effect of the precipitates on the appearance of the R-phase and suppression of the direct transformation from A to M.

Thanks to their particular properties, NiTi and NiTi-based alloys have been widely used in several engineering applications. From medical implants and devices in the biomedical field to actuators in the automotive and aerospace. But they are also used as micro-electromechanical systems (MEMS), for electrical circuit protections in electrical devices, in the energy field for heat engines and even in the artist community as actuation for sculptures [7]. Designing all these devices correctly is crucial to ensure mechanical strength, reliability and performance. Typically, two complementary approaches are considered: experimental and computational. The former bases the design on experimental analysis and typically on a try and error approach, while the latter focuses on parametric numerical studies of the device. Computational models are becoming an essential tool in the design process, saving time and allowing the investigation of parameters which are typically unmeasurable in experimental setup. To properly represent the complex behavior of a SMA, such as NiTi, two main approaches have been followed: phenomenological and micromechanical. While the former aim to fit experimental data determining parameters then used in the constitutive models, the latter focused on the behavior of the microstructure of the alloy and results to be more complex and computationally demanding [8, 9]. Among the several constitutive models developed to mimic the behavior of a SMA, it is worth to highlight the model of Tanaka [10] which was then improved by several authors [11, 12] and the phenomenological model of Auricchio et al. [13, 14], also improved over the years. Besides the differences in the constitutive models developed by the above-mentioned researchers, all the computational models present common parameters like the transformation temperatures and the slope of the transformation stress-temperature curves, which are fundamental in the experimental design approach as well. The latter parameter is typically known as Clausius-Clapeyron coefficient (*CCC*) and is modeled by the Clausius–Clapeyron equation [15–17]:

$$\frac{\mathrm{d}\sigma}{\mathrm{d}T} = -\rho\frac{\Delta S}{\varepsilon_{\mathrm{t}}} \tag{1}$$

where ρ is the density of the transforming body, ε_{t} is the transformation strain, ΔS is the entropy change. The thermoelastic martensitic transformation of NiTi is both a mechanical (PE) and a thermal process (SME). The Clausius–Clapeyron equation has been specifically developed to express the linear relationship between stresses and temperatures and as stated before, the *CCC* is used as a constant parameter for numerical model and mechanical design.

In the development of a SMA-based device, it becomes fundamental to investigate how heat treatments parameters (temperature and time) affect the thermo-mechanical response of the SMA. Several studies have been already conducted. For example, Wang et al. [18] investigated the effects of both thermal treatment and Ni content on the transformation temperatures and mechanical response of NiTi wires (49.9 at.% Ni–Ti) The aim of that study was to determine a mathematical relationship between the thermo-mechanical history of the alloy and its properties. Similarly, Grassi et al. [19] studied the effect of thermal treatment on the mechanical behavior of NiTi mini coil springs. They investigated the change in stiffness of the springs as a function of thermal treatment time and temperature. Liu et al. [20] determined the optimal heat treatment parameters to obtain desired mechanical properties for body temperature applications. Using 50.7 at.% Ni–Ti wires they noticed a slight increase in *Af* with treatment time, for all the temperatures of the process and an overall decrease in the upper and lower plateau stress with aging time, for a tensile test performed at 37 °C. Similar results were also obtained by other research groups [21–23]. Finally, we also want to highlight the study of Zhan et al. [24] where the effect of both thermal treatment and percentage of cold work was studied on binary NiTi (49 Ni–51Ti at.%). From the results of that study, it has been noticed a decrease in the transformation temperature with the decrease of HT temperature, particularly marked for high percentage of cold work.

Nevertheless, to our knowledge, none thorough study has been conducted to investigate how the Clausius-Clapeyron coefficient is affected by the HT temperature and time on binary NiTi wires. In order to fill this gap, the aim of this study is to determine how the Clausius-Clapeyron Coefficient (*CCC*) and the Transformation Temperatures are affected by the time and temperature of the thermal treatment. The study is conducted on two different casting batches of commercially available Body Temperature (BT) NiTi alloys. This class of NiTi alloys has been increasingly exploited in the biomedical field since the 1970s. When this field started moving toward medical procedure less invasive, the demand for new devices and so materials, which can overpass the limits of the traditional ones, increased. Commercially available body temperature (BT) NiTi alloys are typically used thanks to their *Af* very close to the human internal temperature together with several advantages inasmuch NiTi shape memory alloy: biocompatibility, high strength and low volume/mass ratio. These properties are exploited in several medical devices like self-expandable stent [25–27], self-closing suture for deep surgical fields [28], angioplasty guidewires [29], percutaneous devices to treat valvular problems and many mores [30–32].

In the present work, the BT NiTi alloys conform to the ASTM F-2063 [33]. This standard shows the general requirements for NiTi alloy with nominally 54.5–57.0 mass% of nickel, for medical field. These specifications are intended for mill product which is then cold worked (drawing) to obtain the desired wire diameter. The effect of the cold work on the thermo-mechanical performances of SMA is lessened by thermal treatment, especially for high temperature and/or time of treatment [24, 34].

Material and methods

Material and heat treatments

Two different casting batches of BT NiTi alloys are here considered: NiTi_1 and NiTi_2. Both alloys conform to the ASTM F-2063. For both materials two wires with different diameter are tested. The first wire is used to study how the martensitic transformation changes based on the HT parameters and to compare NiTi_1 with NiTi_2, while the second wire is used to assess the replicability of the results, ensuring that the wire diameter (and so the percentage of cold work) does not affect the observed outcomes. For NiTi_1, the following two diameters were available: 150 µm (NiTi_1–150) and 200 µm (NiTi_1–200), where the first one is used to study the effect of the heat treatment and the second to assess the replicability of the test. For NiTi_2 a 400 µm wire (NiTi_2–400) is used for the main study and a 300 µm wire (NiTi_2-300) for the replicability check. All the wires are subjected to a thermal treatment conducted in a resistive furnace in no-controlled atmosphere. To evaluate the effect of the HT on the thermo-mechanical performance of the BT wires, thermal treatments were conducted considering different temperatures and times. Here are considered seven treatment temperatures (from 573 to 873 K with a step of 50 K) and 6 treatment times (from 15 to 90 min with a step of 15 min). After the HT, specimens follow a quench in water at room temperature. Only the wires used to study the effect of the HT on the thermo-mechanical response of the material (NiTi_1–150 and NiTi_2–400 wires) are subjected to all HT times and temperatures, while the ones used to assess the replicability of the test (NiTi_1–200 and NiTi_2–300 wires) are treated only for significant ones: 673,723,773 and 823 K as HT temperatures and 30 and 60 min as HT times. Table 1 lists all the heat treatments performed on each wire.

Table 1 Table resuming all the temperatures and times of treatment used for both NiTi_1 and NiTi_2 wires

Sample	HT Temperature/K	HT Time/min
NiTi_1–150	573,623,673,723,773,823,873	15,30,45,60,75,90
NiTi_1–200	673,723,773,823	30,60
NiTi_2–400	573,623,673,723,773,823,873	15,30,45,60,75,90
NiTi_2–300	673,723,773,823	30,60

Differential scanning calorimetry

Solubilized samples (1073 K for 15 min with final water quench) are analyzed through differential scanning calorimetry, DSC (DSC25 TA instruments, New Castle, DE, USA), to assess the inhomogeneity between the two batches of NiTi samples and homogeneity within the same batch.

Therefore, DSC is employed to evaluate the effect of the selected thermal treatment (see Table 1) on the phase transformation temperatures. For all specimens, we focus on the *Af* and *Rs*. The test is performed from 183 to 393 K with a heating/cooling rate of 5 K min^{-1}. *Af* and *Rs* are identified from the DSC curve through the tangent method at the endothermic and exothermic peak, respectively.

Strain recovery test

CCC is evaluated through strain recovery (SR) tests. For this analysis a Q800 TA instruments (New Castle, DE, USA) equipped with a liquid nitrogen cooling system is used. The SR test is performed in tension at three levels of stress 50, 100 and 150 MPa with the exception of NiTi_2–400 wire which is tested at 50, 100 and 140 MPa, for machine limitations. At each stress level, the sample is subjected to a thermal cycle from 153 to 393 K with a heating/cooling rate of 5 K min^{-1}. From the SR curves the transformation temperatures (*As*, *Ms*, and *Rs*) are identified through the tangent method. Once obtained the transformation temperatures for each stress level, they are plotted (on the x-axis) with respect the stress level (on the y-axis). The data are then linearly interpolated and the *CCC* [$MPaK^{-1}$] is therefore evaluated as the slope of that curve. SR is performed on all samples except for the NiTi_1–200 and NiTi_2–300 wires treated at 823 K for both 30 and 60 min and the NiTi_1–150 and NiTi_2–400 wires treated for 75 and 90 min at all considered HT temperatures.

Results

Compared to Gall et al. [35], in this work no study of the microstructure of the two alloys, through optical analysis, is conducted to correlate the changes in the microstructure and the presence of precipitates with the thermal behavior of the alloy.

Phase transition temperatures of the casting batches

Figure 1 reports the DSC curves of the solubilized samples. It can be observed that the DSC curves completely overlaps within a same batch. On the other side, significant differences are noticeable between the DSC curve of samples of the two casting batches. From these curves the transformation temperatures for both NiTi alloys are obtained. In particular, it is obtained *Af* equal to 310 K and 292 K and *Ms* equal to 269 K and 282 K, respectively, for NiTi_1 and NiTi_2. According to the work of Nespoli et al. [36] and Frenzel et al. [37], it is possible to estimate the atomic composition of the NiTi alloy from the transformation temperatures of the solubilized material. By exploiting the curves representing the influence of Ni concentration on the transformation temperatures of the alloy, reported in [36] and [37], it is determined a 50.5 at.% Ni for NiTi_1 and 50.6 at.% Ni for NiTi_2. Finally, from the DSC curves of Fig. 1 it is obtained the value of enthalpy change for both casting batches, with 20.24 J g^{-1} for NiTi_1 and 18.33 J g^{-1} for NiTi_2.

Phase transition temperatures *vs* Heat treatment

Figures 2 and 3, respectively, report the value of *Af* of NiTi_1–150 and NiTi_2–400 wires as a function of the temperature and time of the thermal treatment. In both cases it is observed a decrease of *Af* between 623 and 773 K HT treatments, regardless HT time. Furthermore, a slightly increase in the transformation temperature for both casting batches is observed between 573 and 623 K HT temperatures. Finally, for thermal treatment temperatures higher than 773 K the behavior changes based on the alloy considered. NiTi_1 presents an increase in *Af* regardless HT time. Instead, NiTi_2, for HT time higher than 45 min, presents an increase in *Af*

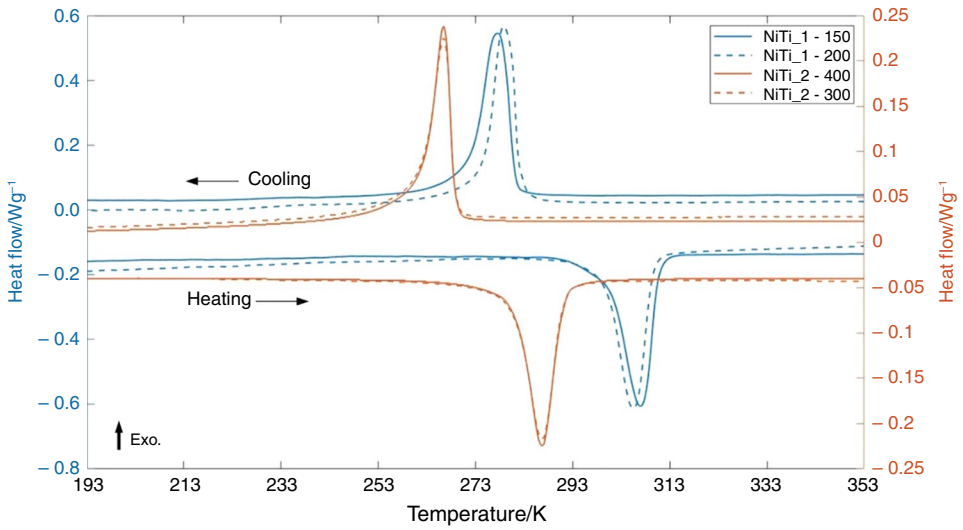

Fig. 1 Curves derived from the DSC analysis on the solubilized samples of NiTi wires

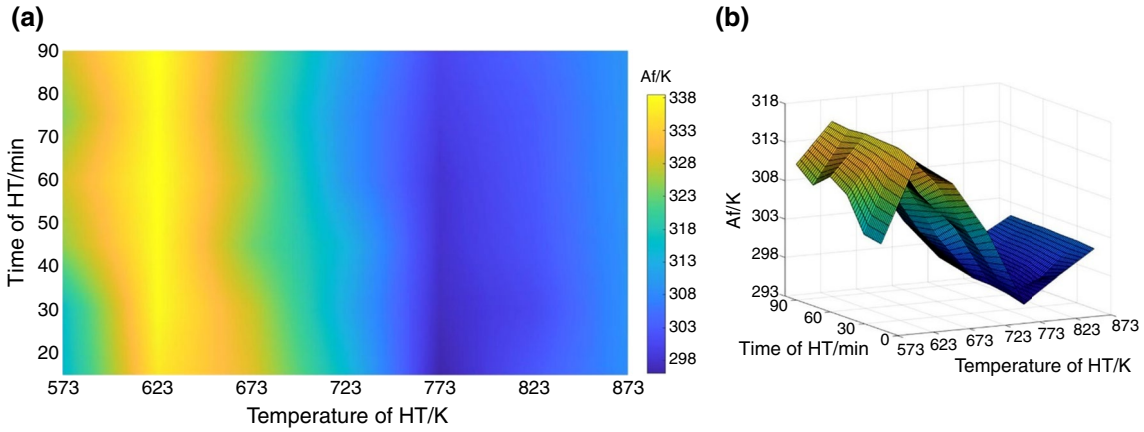

Fig. 2 *Af* as a function of HT temperature and time for the NiTi_1–150 wire: **a** 2D Colormap of *Af* and **b** 3D colormap of *Af*

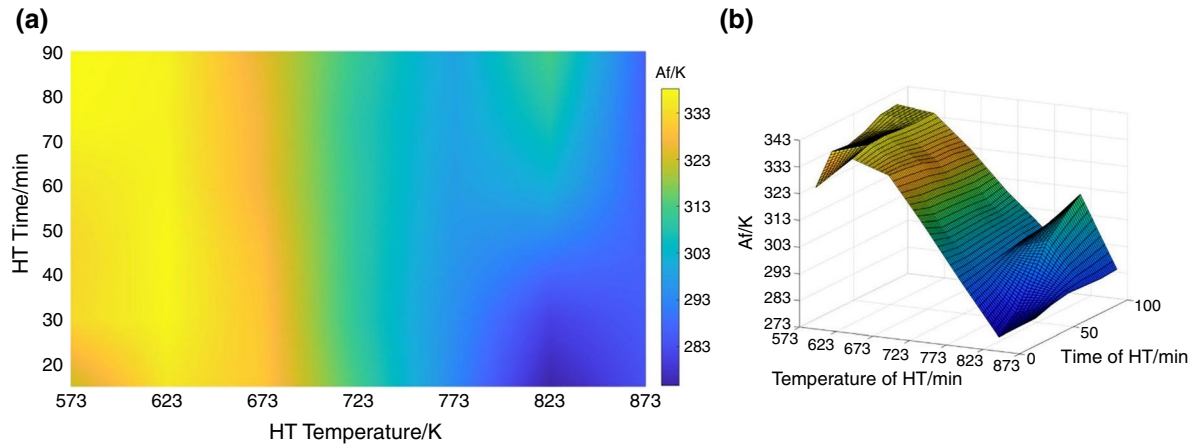

Fig. 3 *Af* as a function of HT temperature and time for the NiTi_2–400 wire: **a** 2D Colormap of *Af* and **b** 3D colormap of *Af*

Table 2 Table resuming the values of *Af*/K as a function of HT temperature and time for the NiTi_1–150 wire

		HT Temperature/K						
		573	**623**	**673**	**723**	**773**	**823**	**873**
HT Time/min	**15**	315	336	329	315	296	303	309
	30	316	338	328	313	297	301	309
	45	325	338	324	314	298	302	309
	60	328	338	326	310	298	303	310
	75	324	338	324	309	299	303	309
	90	328	339	325	311	300	304	310

up to 773 K HT temperature followed by a decrease, while for HT times lower than 45 min it shows the exact opposite behavior. No significant fluctuations in *Af* are observed when HT time is changed for the same temperature of treatment,

Table 3 Table resuming the values of *Af* /K as a function of HT temperature and time for the NiTi_2–400 wire

		HT Temperature/K						
		573	**623**	**673**	**723**	**773**	**823**	**873**
HT Time/min	**15**	322	335	330	312	293	275	283
	30	331	337	330	309	294	281	285
	45	332	337	329	309	296	291	287
	60	334	337	326	310	297	302	286
	75	338	336	326	309	299	308	286
	90	338	337	325	311	299	313	287

except for the NiTi_2–400 wire treated at 823 K, where moving from 15 to 90 min of treatment determines a change in *Af* from 275 to 313 K. Even if it is slighter than the NiTi_2–400 treated at 823 K, also for NiTi_1–150 and NiTi_2–400 heat treated at 573 K it is noticed an increase in *Af* moving from 15 to 90 min HT time. In particular, for the NiTi_1 wire it is observed an increase from 315 to 328 K while for the NiTi_2 from 322 to 338 K. This result could be partially associated to a high rater-dependency on the detection of *Af* due to the twisting path of DSC curves. Tables 2 and 3, respectively, resumed all the values of *Af* obtained from the DSC analysis as a function of HT temperature and time of the NiTi_1–150 and the NiTi_2–400 wires.

Figure 4 shows the 3D surfaces of *Af* as a function of HT temperature and time for the NiTi_1–150 wire in Red-based color scale and the NiTi_2–400 wire in Gray-based color scale. The two batches of casting present the same overall trend of *Af* as a function of HT temperature and time, with some regions of the plane where the values of transformation temperature present a negligible difference (between 623 and 773 K HT temperature) and regions where the behavior of the two materials diverges (for HT temperatures lower than 623 K and higher than 773 K). In particular, it is obtained a difference always lower than 5 K between 573 and 773 K HT temperatures, while for HT at a temperature higher than 773 K, the difference between the two wires is not negligible, reaching values of almost 30 K (Fig. 5). Finally, for HT temperatures lower than 623 K, could be observed differences up to almost 15 K which could be associated not only to the material but also to the remaining effect of cold work. For thermal treatment at higher temperatures, the effect of the cold work is reduced and the difference is totally ascribable to the material.

Figure 6a and b compares the values of *Af* between the NiTi_1–150 and NiTi_1–200 and between NiTi_2–400 and NiTi_2–300 wires, respectively. This comparison is

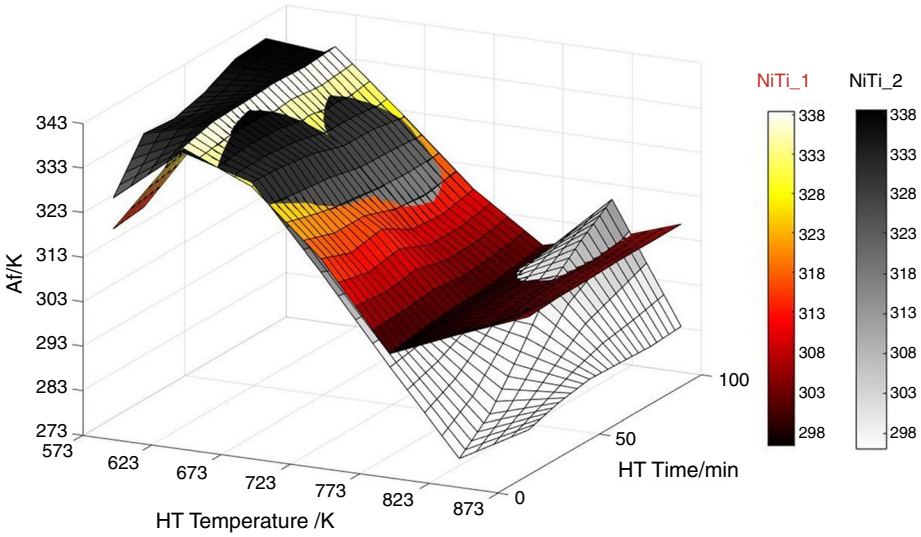

Fig. 4 Comparison by superimposition of the 3D surfaces representing the value of *Af* as a function of HT temperature and time for NiTi_1–150 and NiTi_2–400 wires. The Red-based colormap represents the NiTi_1–150 wire while the Gray-based colormap is for the NiTi_2–400 wire

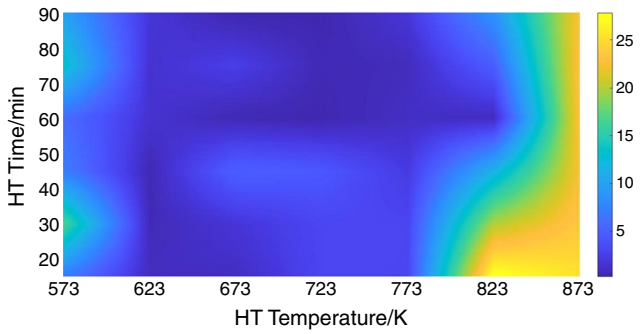

Fig. 5 Absolute difference between *Af* value of NiTi_1–150 and NiTi_2–400 wires

carried out to check that the wire diameter is not affecting the outcomes, allowing to assess that the difference observed between NiTi_1 and NiTi_2 is totally ascribable to the material. As can be seen from Fig. 6a and b, no significant difference is obtained in terms of *Af* between the wires of the same casting batch. The only slight difference is observed between the NiTi_2–300 and the NiTi_2–400 wires for thermal treatment temperatures lower than 623 K, associable to the remaining effect of cold work. Figure 6c and d presents the values of absolute temperature difference between wires of the same casting batch, 400 µm *vs* 300 µm and 150 µm *vs* 200 µm, respectively. In both cases, the difference is always lower than 5 K. In particular, for NiTi_1 the difference reaches at least 3 K for heat treatment at 673 K for 60 min. From the previous presented results, it is possible to confirm the replicability of the DSC analysis. Tables 4 and 5 resume the values of *Af* for the NiTi_1–200 and NiTi_2–300 wires, respectively.

Besides the effect of the HT temperature and time on the value of *Af*, it is possible to study its effect on *Rs*. Figures 7 and 8, respectively, show *Rs* as a function of HT time and HT temperature for NiTi_1 (Figs. 7a and 8a) and NiTi_2 (Figs. 7b and 8b). This result is shown for all HT temperatures with the exceptions of 873 K, due to the fact that single-stage transformation occurs for this treatment temperature, and of 573 K, due to difficulties in the detection of the *Rs* from the DSC curves. For NiTi_1, the *Rs* does not present a significant dependence on the HT time for every HT temperature considered between 623 and 823 K. Similarly, for NiTi_2 the value of *Rs* results to be almost insensitive to the change of the HT time for all HT temperature but for 823 K, for which it increases from 268 to 298 K spanning from 15 to 90 min of heat treatment. On the other hand, *Rs* presents an interesting trend with the HT temperature, see Fig. 8. The two alloys present a linear trend of Rs with HT temperature that is independent from HT time. In particular, from 623 to 773 K it occurs an overall decrease of almost 70% and 68% in *Rs* for NiTi_1 and NiTi_2, respectively.

CCC vs heat treatment

Figure 9 reports two examples of SR curves for NiTi_2–400 treated at 573 K for 15 min (Fig. 9a) and at 773 K for 60 min (Fig. 9b). Figure 9 highlights the difference in curve's shape generated by the SR test on wire treated at different temperatures and times. In particular, low HT temperatures and HT times results in poorly shape curves which generate a high rater-dependence on the measure of the transformation temperatures. It is worth to highlight the presence of the R-phase under cooling for the wire treated at 773 K for 60 min (Fig. 9b), characterized by the presence of two steps. From the SR curves, like the ones shown in Fig. 9, the value of *CCC* is obtained as described in the Material and Method section. The *CCC*

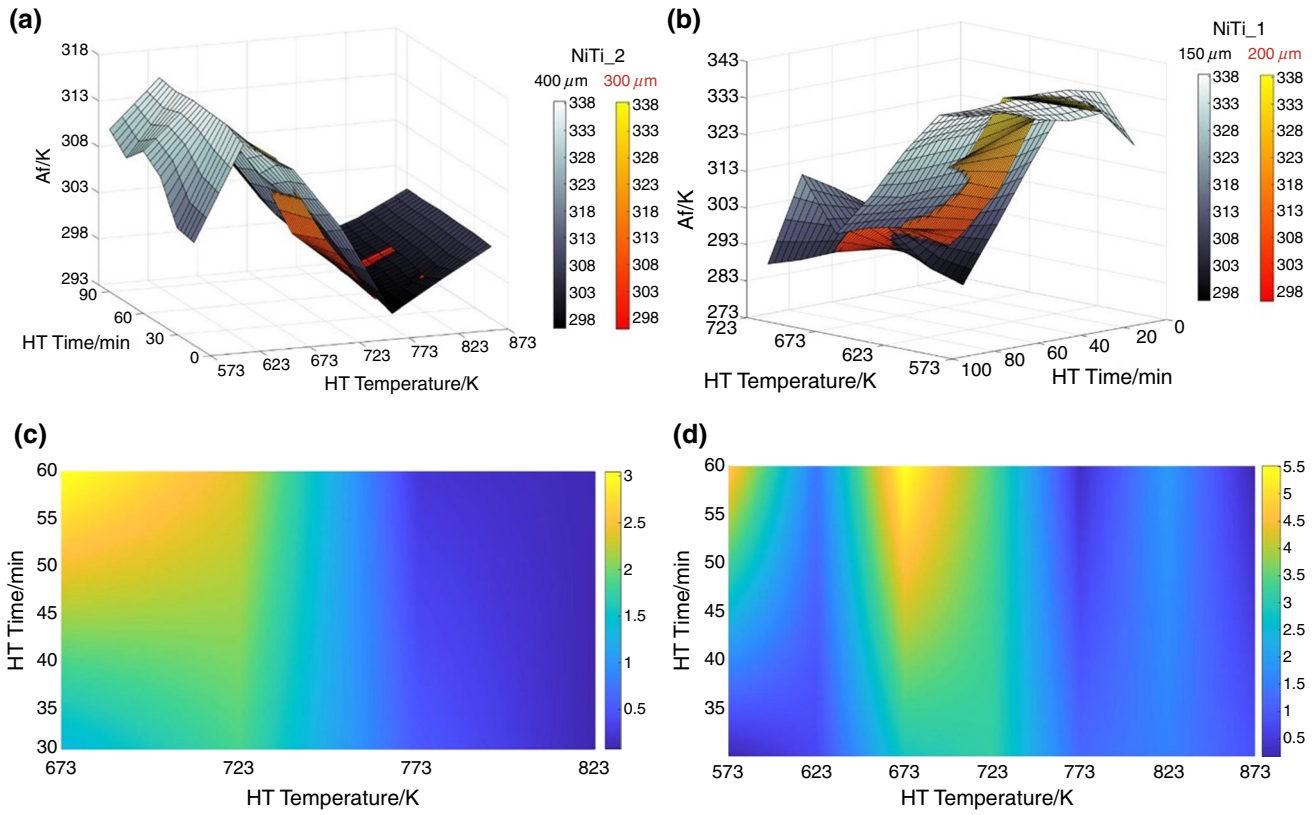

Fig. 6 Comparison by superimposition of the 3D surfaces representing the value of *Af* as a function of HT temperature and time between NiTi_1–150 and NiTi_1–200 (**a**) and between NiTi_2–400 and NiTi_2–300 (**b**). Absolute difference in the value of *Af* evaluated between NiTi_1–150 and NiTi_1–200 (**c**) and between NiTi_2–400 and NiTi_2–300 (**d**)

Table 4 Table resuming the values of *Af*/K as a function of HT temperature and time for NiTi_1– 200 wire

		HT Temperature/K			
		673	**723**	**773**	**823**
HT Time/ min	**30**	329	311	297	301
	60	329	307	298	303

values of NiTi_1 and NiTi_2 BT wires are shown through flat color maps, with HT temperature on the x-axis, HT time on the y-axis and value of *CCC* expressed through a graduated color scale.

Table 5 Table resuming the values of *Af*/K as a function of HT temperature and time for NiTi_2–300 wire

		HT Temperature /K						
		573	**623**	**673**	**723**	**773**	**823**	**873**
HT Time/ min	**30**	333	337	327	306	293	299	285
	60	339	338	321	313	300	300	287

NiTi_1 BT wires

Considering the NiTi_1–150 (Fig. 10), the value of *CCC* does not follow a specific and repeatable trend for the considered transformation temperatures. As regard *As* (Fig. 10a), the value of CCC presents a behavior slightly dependent on the HT time, with an initial decrease as a consequence of an increase in HT temperature from 573 to 723 K. For HT temperatures from 723 to 823 K the *CCC* value of *As* increases again reaching a maximum in 823 K, where it starts decreasing down to a minimum in 873 K HT temperature. *CCC* of *Ms* (Fig. 10b) shows a rise from 773 to 873 K HT temperatures, particularly sharp between 823 and 873 K. Instead, spanning from 673 to 773 K HT temperatures, it occurs a slight reduction in the value of *CCC*. Then, between 573 and 673 K, the *CCC* of *Ms* presents small variations with no particular trend, remaining always between 3 and 9 MPa K^{-1}. Finally, the value of *CCC* of *Rs* (Fig. 10c) is evaluated only for the HT temperatures and times which allow to determine the transformation temperature from the SR curves. In particular, for treatment at 573 K the measure of the *Rs* results highly rater-dependent and so the value of *CCC*, thus it is not represented here. Furthermore, for treatments at 823 K and

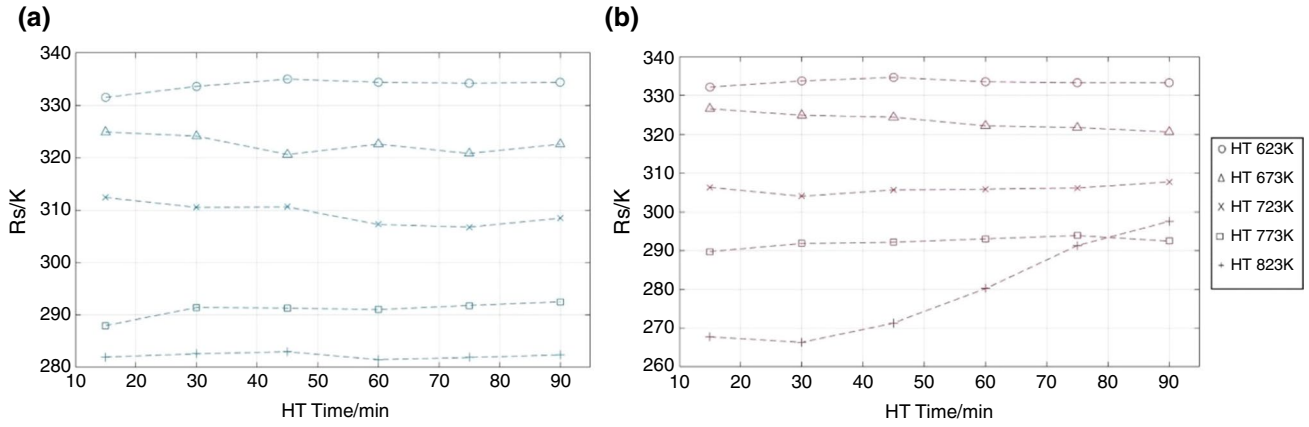

Fig. 7 Transformation temperature *Rs* as a function of the treatment time for HT treatment between 623 and 823 K for both NiTi_1 (**a**) and NiTi_2 (**b**)

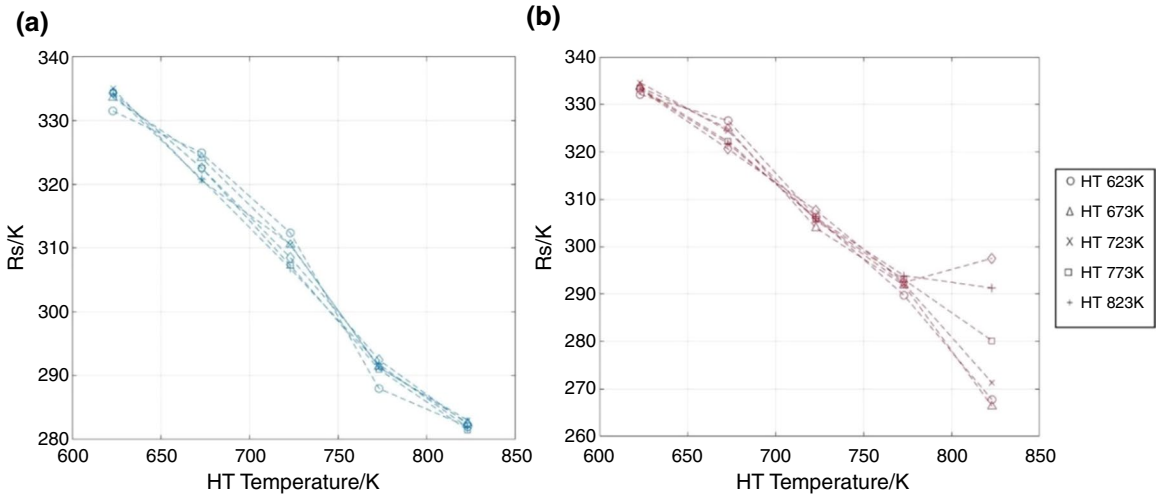

Fig. 8 Transformation temperature *Rs* as a function of the HT temperature for each HT time, for both NiTi_1 (**a**) and NiTi_2 (**b**)

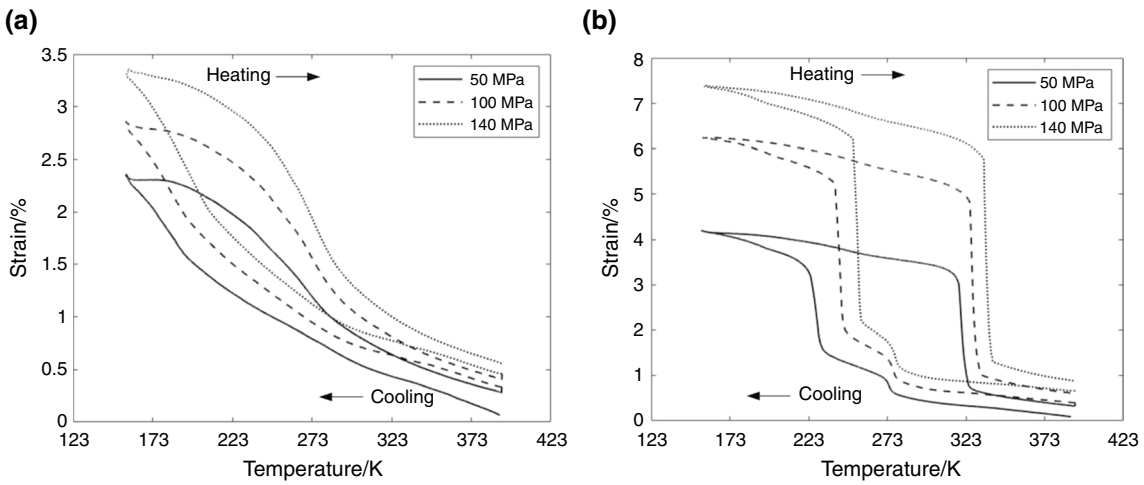

Fig. 9 Curves derived from SR tests on NiTi_2–400 treated at 573 K for 15 min (**a**) and at 773 K for 60 min (**b**). The three stress levels are highlighted through different line style

873 K the *Rs* is not measurable from the SR curve. Thus, it is not possible to obtain the *CCC* value for these temperature of treatment for all HT times. *CCC* of *Rs* presents an overall increase moving from 623 to 673 K. Then the value of *CCC* decreases down to its minimum at 773 K HT temperature. Over HT times for all HT temperatures the value of *CCC* is almost constant with the exception of 673 K of treatment, which presents a significant decrease of *CCC* following an increase in HT time. In general, the value of the *CCC* for *Rs* is always higher than the values obtained for *As* and *Ms* (at equal HT parameters). To assess the replicability of the outcomes, whatever wire diameter considered, the SR analysis is repeated on the NiTi_1–200 wire, only analyzing the values of *As* and *Ms*. The values of *CCC* as a function of HT temperature and times, for both NiTi_1 wires, are compared in Fig. 11. The values obtained from the two wires present a negligible difference, always lower than 0.8 MPa K^{-1}.

NiTi_2 BT wires

Figure 12 reports the color map of the values of *CCC* for the NiTi_2–400 wire, of *As*, *M*s and *Rs* transformation temperatures. For *As* (Fig. 12a) it is observed an increase of *CCC* moving from 873 to 773 K of HT temperatures followed by a decrease down to its minimum at 723 K HT temperature. Then, from 723 to 573 K there is a rise in the value of *CCC*. Regarding the value of *CCC* of *Ms*, the NiTi_1–150 and NiTi_2–400 present similar trends. Finally, for NiTi_2–400 the value of *CCC* of *Rs* presents a similar behavior to NiTi_1, with a peak at 673 K HT temperature. Also for NiTi_2 the second wire diameter (300 μm) is tested to determine whether the percentage of cold work (diameter of the wire) affects the outcomes of the analysis. As it is shown in Fig. 13, the difference in the value of *CCC* as a function of HT time and temperature for the NiTi_2–400 wire and the NiTi_2–300 wire is almost negligible among the whole HT plane. So, the wire diameter does not affect

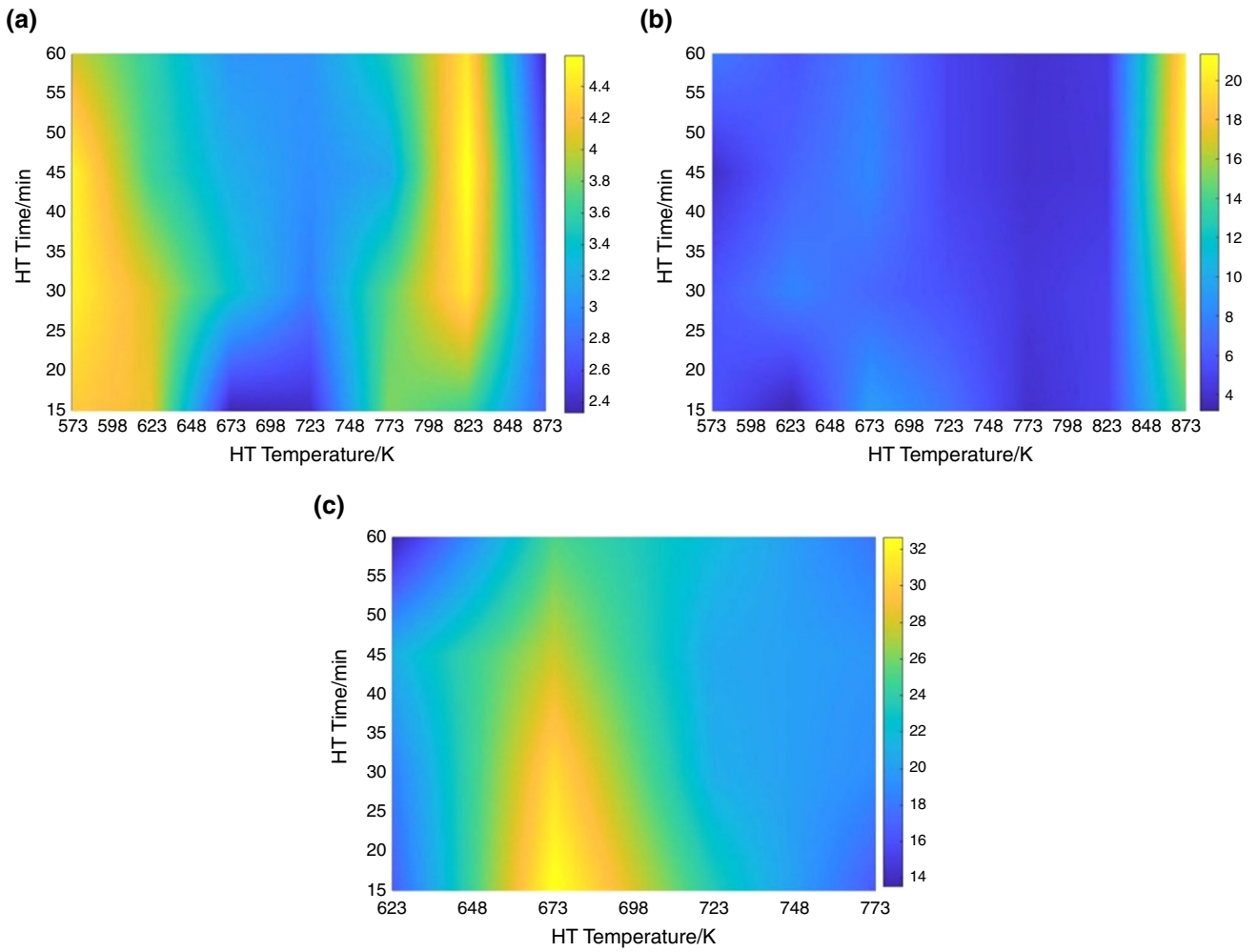

Fig. 10 2D colormap value of *CCC*/MPaK^{-1} of *As* (**a**), *Ms* (**b**) and *Rs* (**c**) as a function of HT temperature and time for NiTi_1–150

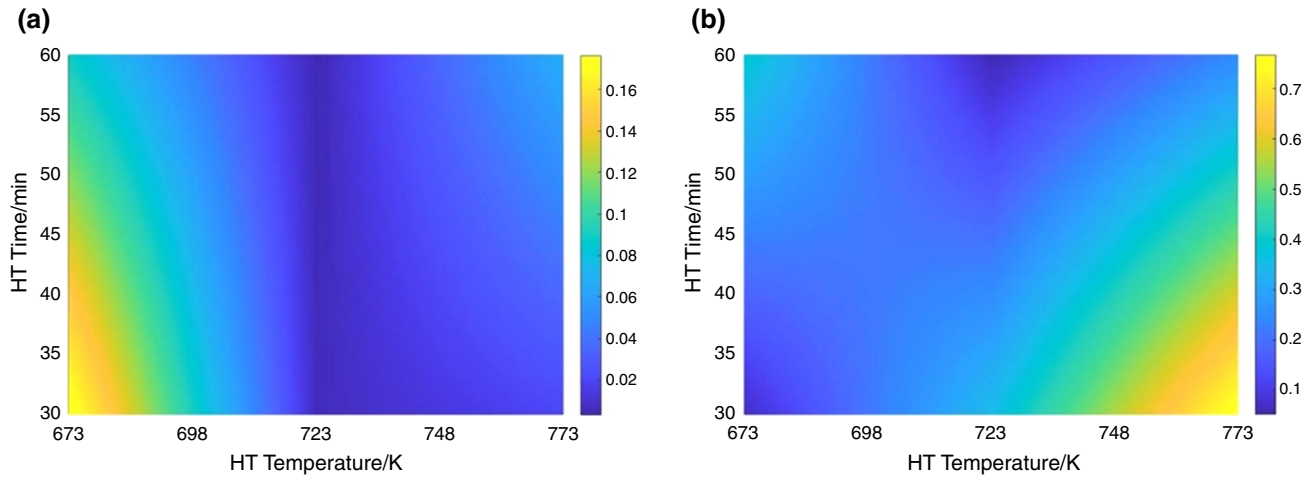

Fig. 11 Difference in the values of *CCC*/MPaK^{-1} of *As* (**a**) and *Ms* (**b**) between NiTi_1–150 and NiTi_1–200 wires

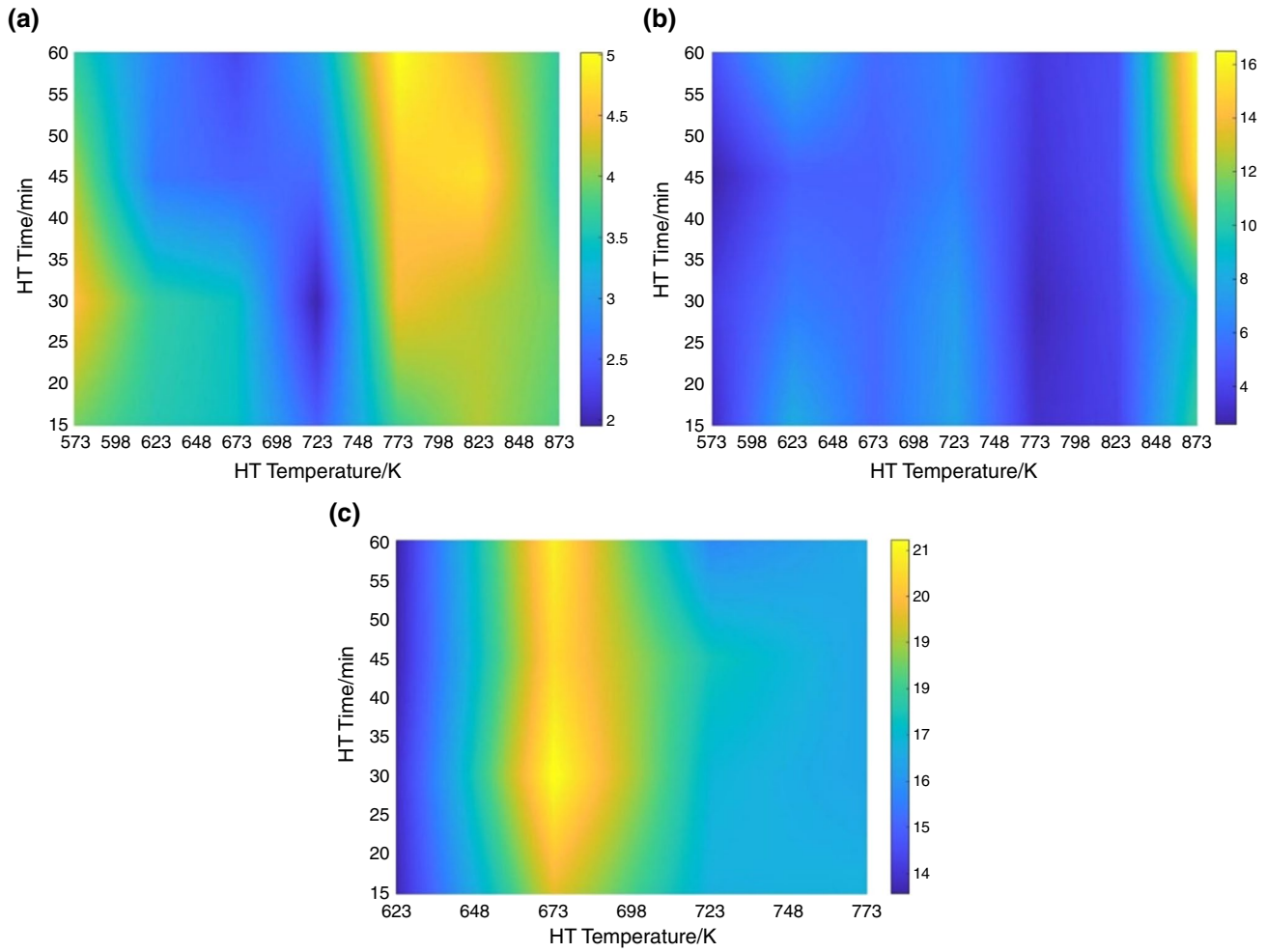

Fig. 12 2D colormap of *CCC*/MPaK^{-1} of *As* (**a**), *Ms* (**b**) and *Rs* (**c**) as a function of HT temperature and time for NiTi_2–400

the values of *CCC*, remaining the same for both 400 and 300 µm wire, which are made of the same NiTi casting batch but different percentage of cold work.

NiTi_1 vs NiTi_2 BT wires

Finally, it is possible to compare the two NiTi casting batches (NiTi_1 and NiTi_2) to determine whether there is a difference in the values of *CCC*. Figures 14 and 15 show the superimposition of the 3D plot of the NiTi_1–150 wire (Gray-based colormap) and the NiTi_2–400 (Red-based colormap) and the absolute difference between the values of *CCC* of the two wires, respectively. As seen above, the two materials present similar trend of *CCC* over the HT time–temperature plane but they present different actual values of the coefficient. For *As*, the difference in *CCC* does not present a particular trend but it is always lower than or equal to 1.5 $MPaK^{-1}$. Instead, for *Ms*, the major difference in *CCC* is obtained for all HT times at HT temperature equal 873 K. Finally, the values of *CCC* of *Rs* of NiTi_1 and NiTi_2 present almost equal trend, but different actual values.

Discussion

Phase transition temperatures of solubilized samples

It is known that the martensitic transformation behavior of binary NiTi alloy is highly affected by the composition of the material. Slightly changes in the Ni content of the NiTi matrix could determine significant changes in the transformation temperatures of the alloy. The two NiTi alloys considered in the present work are derived from two distinct casting batches, thus determining a slight difference in the final composition of the alloy which result in non-identical values of transformation temperatures of the solubilized samples, as visible in the DSC curve of Fig. 1. No difference is observed in terms of DSC curves between the wires obtained from the same casting batches. This is due to the solubilization process which almost nullify the effect of cold work end leads to the total elimination of precipitates. The composition of the two alloys is not determined through a precise chemical analysis of the material but by exploiting curves representing the relationship between Ni content and transformation temperatures of binary NiTi [36, 37]. Through a graphical approach, a content of 50.5 at.% and 50.6 at.% of Ni is estimated for NiTi_1 and NiTi_2, respectively. A more precise chemical analysis should be carried out to verify the approximated composition found in this work.

Effect of heat treatment on the transformation temperatures

One of the main techniques to properly obtain the desired thermo-mechanical characteristics of NiTi alloys consist in heat treatment. In particular, HT time and temperature are the most influential parameters affecting the final behavior of the material. From literature, it is known that in Ni-rich NiTi alloys, such as the ones considered in the present work, heat treatment strongly affects the transformation temperatures of the alloy due to formation of precipitates. Due to the fact that most of precipitates present a Ni-rich composition, their formation brings to a depletion of Ni from the

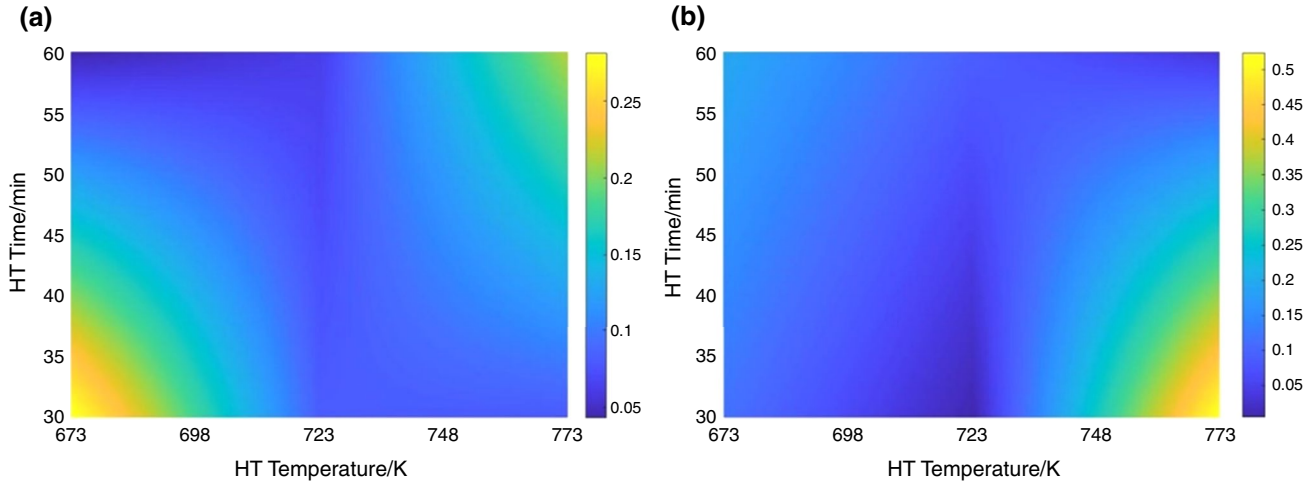

Fig. 13 Difference in the values of *CCC*/$MPaK^{-1}$ of *As* (**a**) and *Ms* (**b**) between NiTi_2–400 and NiTi_2-300 wires

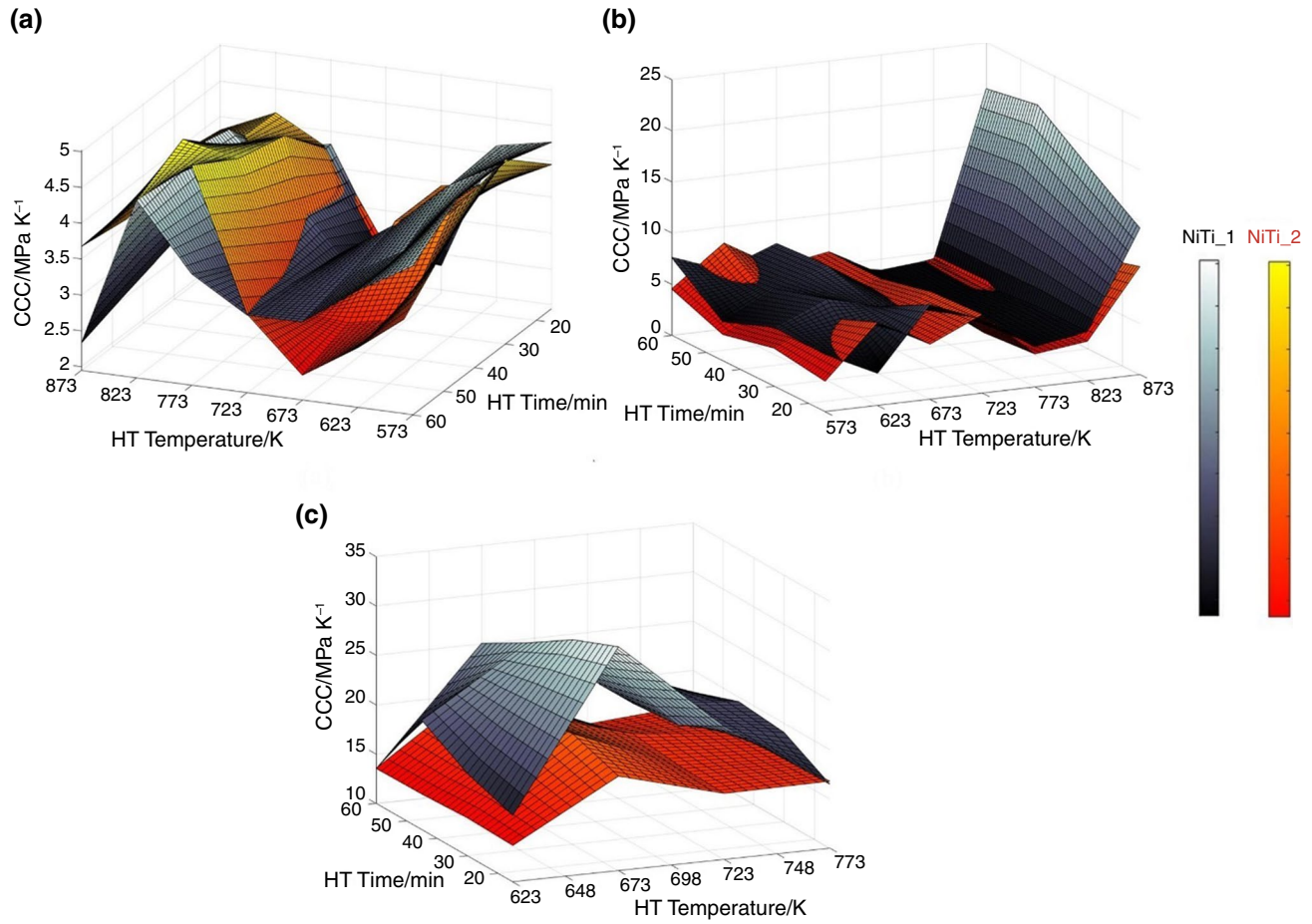

Fig. 14 Comparison by superimposition of the 3D surfaces representing the values of *CCC*/MPaK^{-1} derived from the SR analysis as a function of HT temperature and time. The comparison is done between the NiTi_1–150 wire (Gray-based colormap) and the NiTi_2–400 wire (Red-based colormap) on the *CCC* value of *As* (**a**), *Ms* (**b**) and *Rs* (**c**)

NiTi matrix which strongly affect the transformation temperatures of the alloy. Short time and low temperatures HT promote, especially, the formation of Ni4Ti3, which not only bring to changes in the transformation temperatures but also in the whole transformation path. The presence of this precipitate can suppress the martensitic transformation promoting a two-step transformation, passing through the R-phase [38]. As an example, Fig. 16 reports the DSC curves for NiTi_1–150 (a) and NiTi_2–400 (b) treated for 45 min at HT temperatures from 573 to 873 K. Low temperatures treatments promote the formation of the R-phase during both cooling and heating, leading to a two-stage transformation. Only for HT at 873 K a single stage transformation is present which highlights a complete dissolution of the Ni4Ti3 precipitates in the matrix. This result is in line with the work of Fraj et al. [39], in which the effect of the HT on the thermo-mechanical properties of Ni-rich NiTi (50.67 at.% Ni) conforms to the ASTM F2063 is studied and with the work of Fan et al. [40] that studied how the precipitates affect the behavior of Ni-rich NiTi alloys.

Figures 2 and 3 present the effect of HT temperature and time on the austenite finish temperature (*Af*) of both NiTi_1 and NiTi_2 wires. It is well known from literature that for high HT temperatures the diffusion rate of Ni and Ti atoms, within the alloy structure, is enhanced while the precipitate nucleation is hindered. On the other hand, lower treatment temperatures lead to a difficult diffusion but high nucleation rate [41]. There are intermediate temperatures of treatment which balance the two processes leading to a maximum precipitation rate, typically between 623 and 723 K. This maximum formation of precipitates leads to a local decrease of Ni in the NiTi matrix determining an abrupt increase in the transformation temperatures. In the present studio, the highest *Af* is obtained for HT at 623 K, within the range of temperatures obtained from literature. This result is similar to what was obtained by Pelton et al. [41] and Liu et al. [42]. The former analyzed the effect of the heat treatment on Ti–50.8 at.% Ni, finding a maximum precipitation at 698 K of HT, while the latter studied the 50.7 at.% Ni–Ti alloy for stent application and obtained the maximum precipitation at

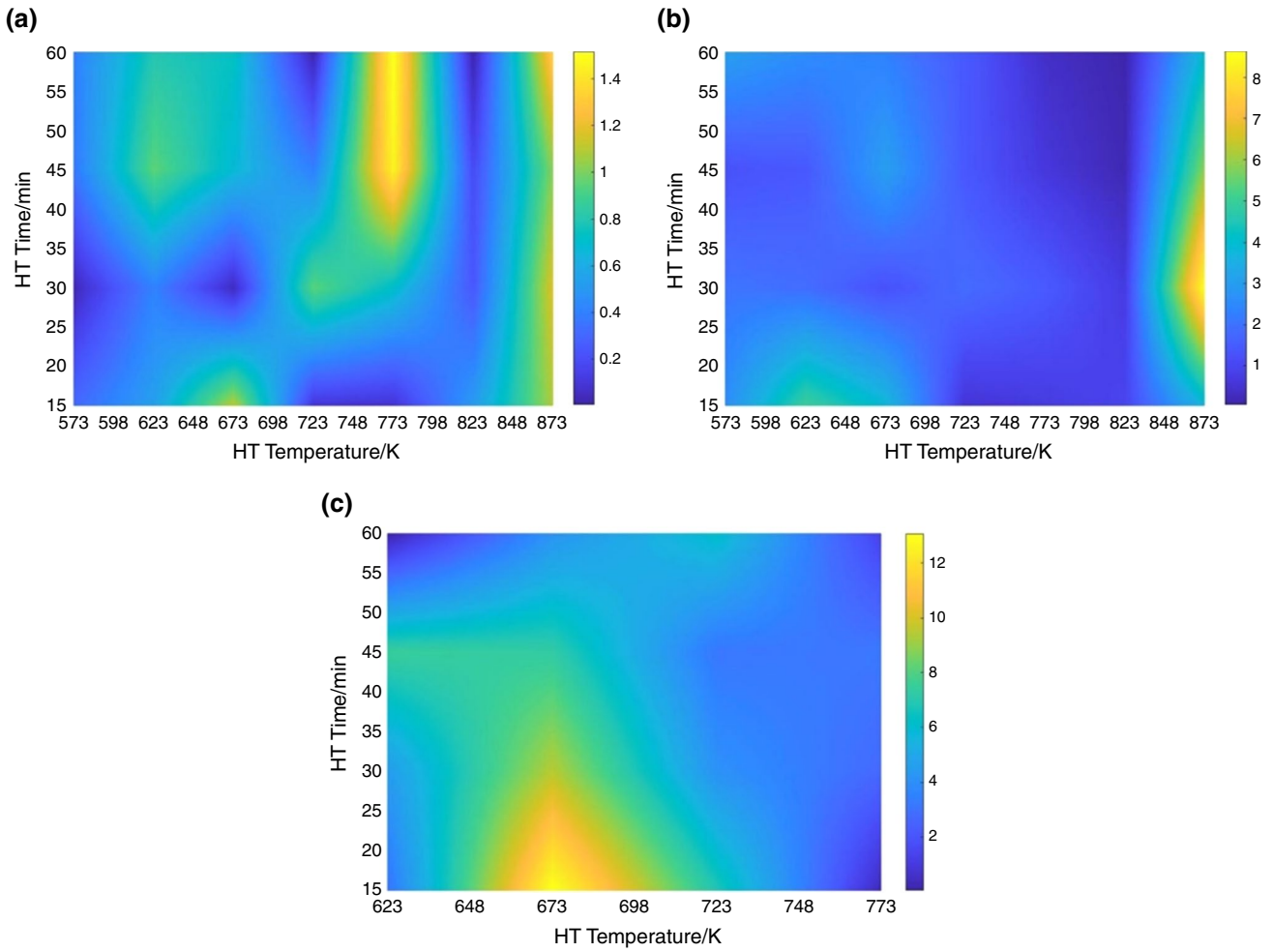

Fig. 15 2D colormap of the absolute difference in CCC/MPaK^{-1} as a function of HT temperature and time between NiTi_1 and NiTi_2 for all transformation temperatures *As* (**a**), *Ms* (**b**) and *Rs* (**c**)

673 K of treatment. It is worth to highlight the difference in atomic percentage of Ni between the alloys considered in the present work (NiTi_1 and NiTi_2) and the alloys considered by Pelton et al. [41] and Liu et al. [42], reminding the estimated values for NiTi_1 and NiTi_2: 50.5 at.% Ni and 50.6 at.% Ni, respectively. By increasing the HT temperature, the Ni4Ti3 precipitates start dissolving and Ni diffuses back into the NiTi matrix. Therefore, the local amount of Ni increases and the *Af* goes down abruptly, as shown in Figs. 2 and 3, reaching the minimum value for HT at 773 K for all HT times for NiTi_1 and 823 K for HT time lower than 60 min and 873 K for HT time higher than 60 min for NiTi_2. For NiTi_2 increasing the HT time for medium–high HT temperatures (above 773 K) leads to higher values of *Af*. This phenomenon could be associated to the formation of Ti2Ni3 precipitate which it has been found to be a metastable precipitate for intermediate temperatures and time of treatment [43]. Ti2Ni3 requires a great amount of Ni to diffuse away from the matrix, leading to a decrease in local Ni content and so a rise in the *Af*. The same phenomenon has been observed by both Pelton et al. [41] and Liu et al. [42] for HT temperature of 823 K. For low HT temperatures (below 773 K) it is observed that HT time has a minor influence on the transformation temperature (*Af*), with values subjected to slighter changes by increasing the time of the treatment. The same behavior has been found also for other NiTi alloys in previous works [41, 42, 44].

It is also worth to highlights the behavior of *Rs* as a function of HT temperature and time. As shown in Fig. 7, the value of *Rs* remains almost constant by increasing the time of the treatment, which mainly affect the density and size of the precipitates in the matrix. Ni4Ti3 represents a strong obstacle for large deformation transformations, such as from R to B19'. While weaker resistance is applied for small deformation transformations like from B2 to R. Therefore, the transformation from A to R results almost insensitive to the density and size of the Ni4Ti3 precipitates, while is highly affected by the local relative variation in

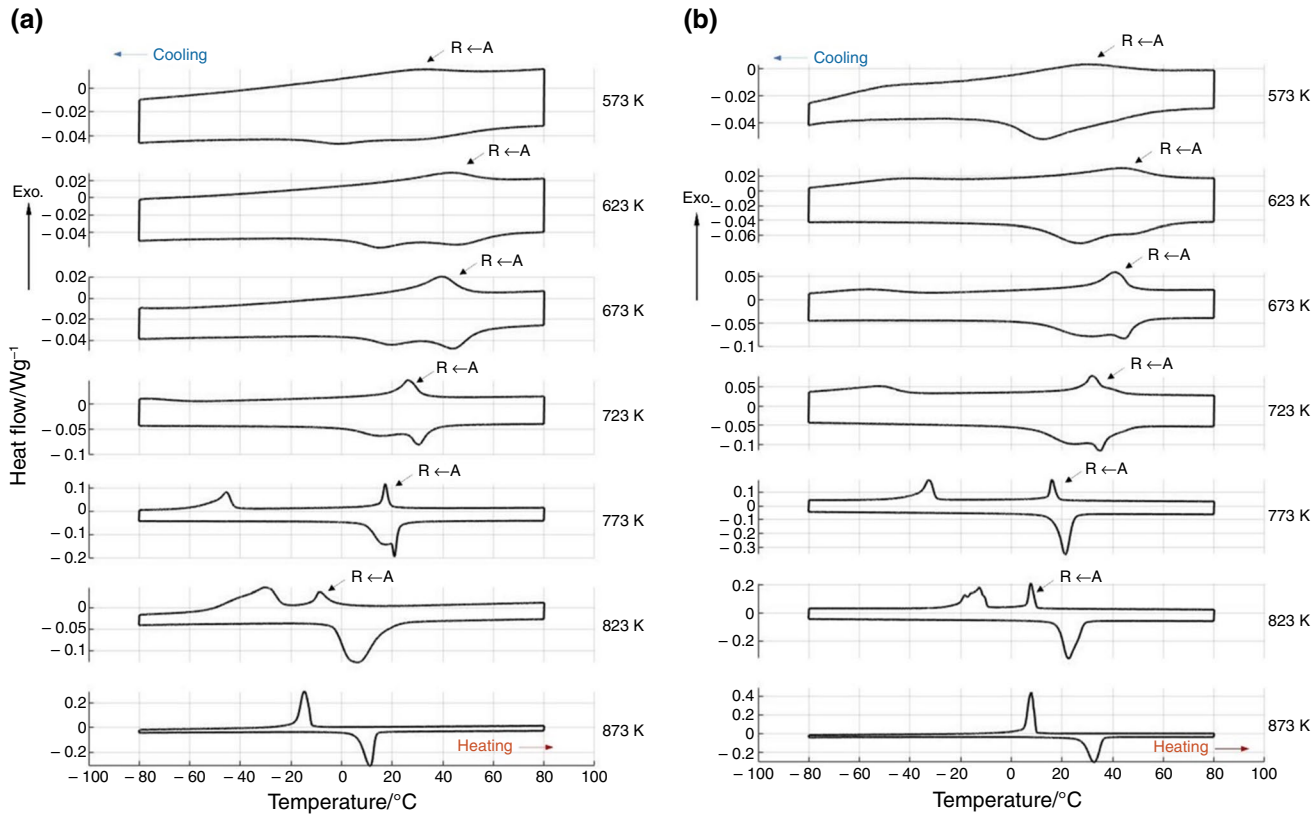

Fig. 16 DSC curves for NiTi_1–150 (**a**) and NiTi_2–400 (**b**) for HT treatment at all temperatures (from 573 to 823 K) for 45 min

the composition of the NiTi matrix. As a matter of fact, *Rs* results practically independent from the HT time, but presents a sharp decrease following an increase in HT temperature. Similar results have been obtained also by Otsuka et al. [45] and Huang et al. [46]. Both studies show a reduction in the value of *Rs* following an increase in HT temperature from 573 to 773 K and from 573 to 973 K, respectively. Finally, comparing the data displayed in Fig. 7a and b, it can be observed that no significant difference exists between the values of *Rs* of NiTi_1 and of NiTi_2. *Rs* results to be strongly affected by the phase equilibrium between B2 and Ni4Ti3 precipitates (local relative variation of the Ni content of the matrix) but almost insensitive to the overall composition of the alloy. Similar results have been obtained from several authors in literature [14, 17, 45–48].

Effect of heat treatment on the CCC

As stated in the introduction of the present work, to properly describe the thermo-mechanical behavior of NiTi alloys or design NiTi-based devices, some parameters, such as the Clausius-Clapeyron coefficient are fundamental. Typically, the *CCC* is used to describe either how the transformation stress changes based on the temperature or how the applied stress affects the transformation temperature of the alloy. As a matter of fact, it could be evaluated through both experimental stress–strain curves at different temperature and strain recovery (SR) tests (as it is done in the present work). Following the former process, the value of plateau stress is obtained as a function of the test temperature. Instead, the latter way involves the measurement of the transformation temperature during iso-stress conditions. According to the work of Duerig et al. [49], to correlate the measurement obtained through SR test with the stress–strain curves method, only some of the transformation temperatures should be considered. In particular, only *Ms* and *As* are expected to be correlated with the upper and lower plateau strength (UPS and LPS), respectively (Fig. 17). The other transformation temperatures (*Af* and *Mf*) could be affected by artifact generated by the lack of thermal quasi-static condition during the heat ramp of the SR test. This is the reason why, in the present work, only *As* and *Ms* are considered. Furthermore, due to very small strain associated to the transformation from A to R, the *R*s is difficulty obtained from SR curves. It would be better to exploit the greater electrical resistivity of the R-phase with respect both A and M and perform electrical resistance measurements. Nevertheless, in the present work the transformation temperature (*Rs*) has been evaluated through SR tests when possible. For low HT

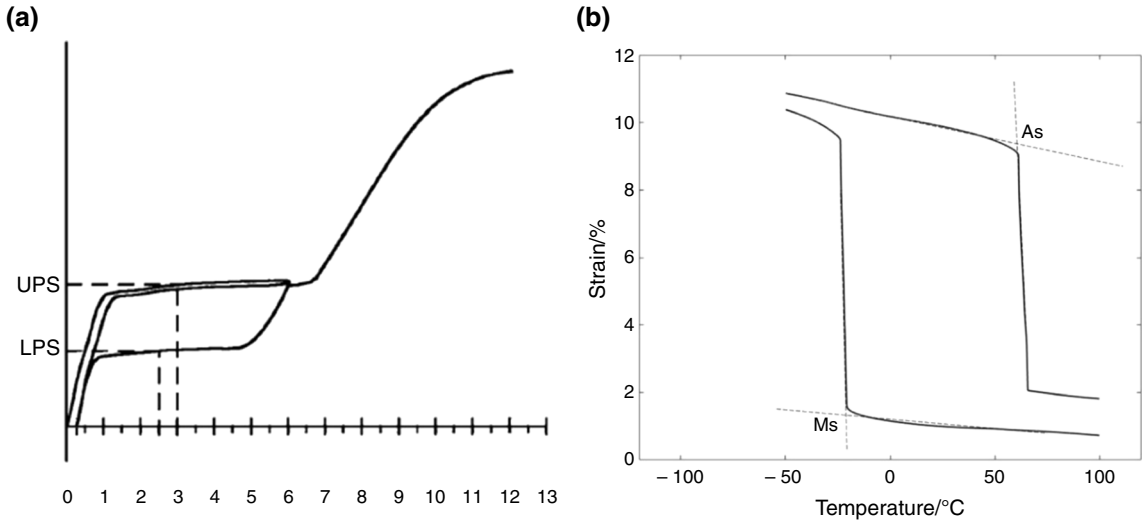

Fig. 17 **a** Stress–Strain curve for the evaluation of UPS and LPS obtained from the ASTM F2516 [50] **b** Strain-recovery curve for the determination of Ms and As

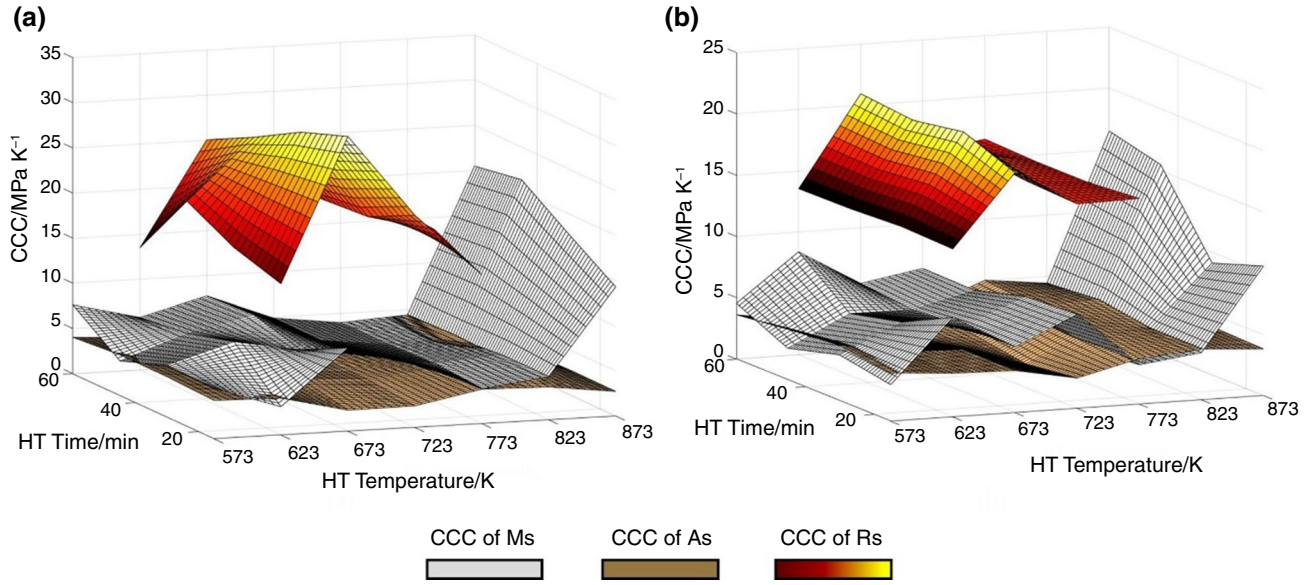

Fig. 18 Comparison of the values of *CCC* of *Ms*, *As* and *Rs* for both NiTi_1 (**a**) and NiTi_2 (**b**)

temperatures and/or low HT times the measure of *Rs* results to be more difficult and highly rater-dependent.

The slope of the stress-temperature curve (*CCC*) is strongly correlated to thermodynamic and mechanical aspects of the NiTi alloy phase transformation. In particular, according to the Clausius–Clapeyron equation (Eq. 1), it is inversely proportional to the relative capacities of the phases to change shape under load ($\Delta\varepsilon$), defined most of the times as "transformation strain". The strain associated to the direct passage from A to M is much higher than the corresponding value considering the passage from A to R. This lower strain value is reflected in a difference in the value of *CCC*. In particular, the obtained values of *CCC* for both NiTi_1 and NiTi_2 for *Rs* are always higher than the corresponding values for *Ms* (Fig. 18). The greater slope of the stress-temperature curve for the R-phase has been observed also by Duerig et al. [49], even if they considered a 50.8 at.% Ni–Ti alloy annealed at 773 K, not analyzing the effect of the thermal treatment on the characteristics of this alloy. Also Liu et al. [51] and Stachowiak et al. [52] found a higher value of *CCC* for the B2 → R transformation with respect the R → B19', for a 50.2 at.% Ni–Ti alloy. It is

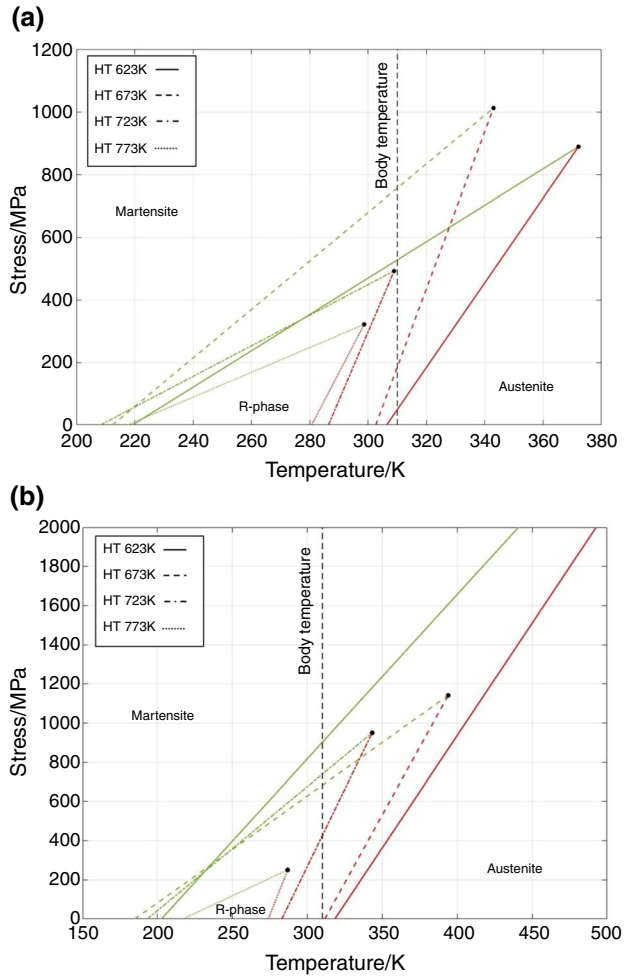

Fig. 19 Stress-Temperature phase diagrams for NiTi_1 (**a**) and NiTi_2 (**b**) treated at different HT temperatures for 60 min. For each HT temperature (different type of hatch) is represented the limit curve from A to R (Red lines) and from R to M (Green lines)

also worth to highlight that the value of *CCC* for *Ms* starts drastically increase for both alloys, approaching the range of values observed only for *Rs*, when the alloy is treated at 873 K. It was shown in the previous section that at this HT temperature the R-phase disappears with complete dissolution of the precipitates. The maximum value of *CCC* of *Rs* occurs, for both alloys, at a HT temperature equal to 673 K (Figs. 10c and 12c). This temperature is close to the HT temperatures range in which the peak of the *Af* has been observed (623–673 K). From the SR analysis results that also the value of *CCC* of *Rs* presents a peak and it occurs in the same range of HT temperatures which leads to the maximum of precipitates, stabilizing the R-phase. Furthermore, the R-phase is observed uniquely under cooling (forward transformation) of the SR test and it could be explained through the principle of irreversible energies [51].

Observing the Clausius–Clapeyron equation (Eq. 1) it is clear that it does not predict a difference in the slope (*CCC*) between the forward (B2 → R → B19' or B2 → B19') and the reverse transformation. However, experimentally a difference in *CCC* is always remarked. In particular, in the present work it is observed an overall higher value of *CCC* for *Ms*, with respect *As*, among the whole HT plane, with pointwise exceptions for NiTi_1 for HT at 823 K for 45 and 60 min and for NiTi_2 for all HT times in the range 773–823 K of HT temperatures. This last trend has been also observed by Fraj et al. [39] on 50.67 at.% Ni–Ti alloy and by Duerig et al. [49] who observed a higher value of *CCC* for the forward transformation for 50.8 at.% Ni–Ti alloy annealed at 823 K.

To the authors' knowledge, no previous study on the effect of the heat treatment on the martensitic transformation of NiTi alloys in terms of *CCC*, has been conducted. Thus, it results difficult to properly compare the behavior of *CCC* among the HT plane with literature data. Nevertheless, to properly understand the importance of considering the effect of the thermal treatment on the martensitic transformation, and as a consequence on the *CCC* it is possible to consider the stress-temperature phase diagrams. These ones shed lights on the competition between the different NiTi phases during the martensitic transformation in relation to the stress-temperature conditions [49]. Figure 19 shows the stress-temperature phase diagrams for both NiTi_1 (Fig. 19a) and NiTi_2 (Fig. 19b) treated at HT temperatures between 623 and 773 K for 60 min. The red and green lines represent the transformation curves from A to R and from R to M, respectively. The point of intersection of these two lines is indicated as the triple point (black dot). Beyond this point, no intermediate R-phase occurs during the martensitic transformation. In Fig. 19 is also represented the body temperature, which is the temperature at which typically these materials work in biomedical applications. It is now clear the effect of the treatment temperature on the martensitic transformation of the alloys. Increasing the HT temperature leads to a reduction of the temperature of the triple point. For NiTi_1, treatments at temperature higher than 723 K for 60 min determine a direct transformation from A to M at body temperature, while lower treatments determine an intermediate passage through the R-phase. For NiTi_2, instead, a HT at 723 K is not sufficient to suppress the R-phase at body temperature, due to the high number of precipitates formed during the heat treatment, as already seen in the previous discussion. The *CCC* of *Rs* results to be the major parameter affecting the temperature value of the triple point. Figure 19 represents only the phase diagram for the forward transformation for a specific HT time. Furthermore, the transformation curve beyond the triple point has not been captured. Further analysis should be conducted to determine the whole stress-temperature phase diagram.

Effect of heat treatment on different diameter wires

As previously discussed, the diameters of the wires considered in this work do not influence the outcomes of both DSC and SR analyses. This result is also explained by considering the heat conduction in cylindric bars. From the geometric dimensions of the specimen, which is a cylindric wire with radius (R) equals to 75, 100, 150 and 200 μm and length (L) about 20 cm, it is possible to determine the characteristic length (L_c) of the sample as:

$$L_c = \frac{V}{A} = \frac{\pi R^2 L}{2\pi RL} \tag{2}$$

Then, by knowing the thermal conductivity (K) of the material and the heat transfer coefficient (h) of the environment, the Biot number (Bi) can be evaluated as:

$$\mathrm{Bi} = \frac{hL_c}{K} \tag{3}$$

If $\mathrm{Bi} < 0.1$ the lumped thermal capacity model can be considered, assuming that the difference in temperature within the sample is almost negligible. It means that during the heat treatment the material is uniformly heated in all points and no spatial gradient is present. By considering the heat transfer coefficient of air from 2.5 to 25 (W m^{-2} °C^{-1}) and a thermal conductivity of NiTi from 5 to 20 (W m^{-12} °C^{-1}), for all diameters it is obtained always a $\mathrm{Bi} < 0.1$. So, it can be assumed that for the considered diameters, the heat treatment equally modifies the microstructure and so the thermo-mechanical properties of the two wires of the same casting batch of NiTi and that explains why no difference is observed.

Conclusions

The phase transition temperatures and the Clausius-Clapeyron coefficient are of great importance for the design of SMA-based devices. Besides the investigation of HT parameters on the transformation temperatures of BT alloys, for the first time in this work has been studied also the effect on the Clausius-Clapeyron coefficient. With respect previous studies which considered high HT times, here HT times lower than 1 h have been examined. The main results of this work are summarized as follow:

- From the DSC analysis it is possible to conclude that both NiTi alloys (NiTi_1 and NiTi_2) present an increase in *Af* for all HT time moving from 773 to 623 K with a peak at 623 K of HT. However, the trend of *Af* for HT treatments higher than 773 K is different between the two casting batches.
- HT time has a minor influence on the value of *Af* with respect HT temperature which affects the formation of precipitates into the NiTi matrix, with subsequent variation in the local composition of the alloy. For treatment higher than 823 K, the dissolution of the precipitates occurs resulting in the suppression of the intermediate R-phase.
- The slope of the stress-temperature curve cannot be considered as a constant for all NiTi alloys, inasmuch it is highly dependent on the thermo-mechanical history of the material.
- The R-phase should not be neglected when low temperatures and times of treatment are considered. Indeed, the appearance of the intermediate R-phase modifies the transformation path affecting the final behavior of the alloy (Fig. 19).
- The wire diameter does not influence the phase transformation temperatures and the Clausius-Clapeyron coefficient for the same casting batches.
- Two different casting batches of the same commercially available body-temperature NiTi alloy wires have been compared in this work. Even if they both are conformed to the same requirements for the NiTi SMA for medical applications, the behavior in terms of *CCC* and phase transformation temperatures present not negligible differences. To properly design a SMA-based device or develop a computational model, it is important to remember that commercially equal NiTi alloy could present remarkable differences in terms of transformation temperatures and *CCC* as a function of HT temperatures and times. The ASTM covers a high range of Ni concentration, but a slight change in it can drastically affect the thermo-mechanical response of the alloy.

Authors' contributions DN: Data curation; Formal analysis; Investigation; Methodology; Validation; Roles/Writing—original draft; Writing—review & editing. FP: Funding acquisition; Resources; Writing—review & editing. AN: Conceptualization; Investigation; Methodology; Resources; Supervision; Validation; Roles/Writing—original draft; Writing—review & editing.

Declarations

Conflict of interest The authors have no relevant financial or non-financial interests to disclose.

References

1. Mohammed MA, Aljubouri AAA, Mhammed SH. Preparation and characterization of equiatomic NiTi shape memory alloy. IOP Conf Ser Mater Sci Eng. 2020. https://doi.org/10.1088/1757-899X/757/1/012059.
2. Oliveira JP, Miranda RM, Fernandes FMB. Welding and Joining of NiTi shape memory alloys: a review. Prog Mater Sci. 2017;88:412–66. https://doi.org/10.1016/j.pmatsci.2017.04.008.
3. Duerig TW, Bhattacharya K. The influence of the R-phase on the superelastic behavior of NiTi. Shap Mem Superelasticity. 2015;1:153–61. https://doi.org/10.1007/s40830-015-0013-4.
4. Asgarinia F, Hashemi SM, Parvizi S. Heat treatment of NiTi alloys, In: Micro and Nano Technologies, Thomas, S., Behera, A., Nguyen, T.A., editors. Nickel-Titanium Smart Hybrid Materials; 2022. pp. 69–101.
5. Nishida M, Wayman CM, Honma T. Precipitation processes in near-equiatomic TiNi shape memory alloys. Metall Trans A. 1986;17:1505–15. https://doi.org/10.1007/BF02650086.
6. Miyazaki S. Thermal and stress cycling effects and fatigue properties of Ni-Ti alloys. Mater Sci. 1990. https://doi.org/10.1016/B978-0-7506-1009-4.50037-8.
7. Sharma N, Ray T, Jangra K. Applications of Nickel-Titanium Alloy. J Eng Technol. 2015; 5(1):
8. Zhu S, Zhang Y. A thermomechanical constitutive model for superelastic SMA wire with strain-rate dependence. SMS. 2007;16:1696–707. https://doi.org/10.1088/0964-1726/16/5/023.
9. Petrini L, Bertini A. A three-dimensional phenomenological model describing cyclic behavior of shape memory alloys. Int J Plast. 2019;125:348–73. https://doi.org/10.1016/j.ijplas.2019.10.008.
10. Tanaka K. A thermomechanical sketch of shape memory effect: one-dimensional tensile behavior. Res Mech. 1986;18:251–63.
11. Liang C, Rogers CA. One-dimensional thermomechanical constitutive relations for shape memory materials. J Intell Mater Syst Struct. 1990;1:207–34. https://doi.org/10.1177/1045389X9000100205.
12. Brinson CL. One-dimensional constitutive behavior of shape memory alloys: thermomechanical derivation with non-constant material functions and redefined martensite internal variable. J Intell Mater Syst Struct. 1993;4:229–42. https://doi.org/10.1177/1045389X9300400213.
13. Auricchio F, Taylor RL. Shape-memory alloys: modelling and numerical simulations of the finite-strain superelastic behavior. Comput Methods Appl Mech Eng. 1997;143:175–94. https://doi.org/10.1016/S0045-7825(96)01147-4.
14. Auricchio F, Coda A, Reali A, Urbano M. SMA numerical modeling versus experimental results: parameter identification and model prediction capabilities. J Materi Eng Perform. 2009;18:649–54. https://doi.org/10.1007/s11665-009-9409-7.
15. Grassi ENB, Chagnon G, Martinni H, de Oliveira R, Favier D. Anisotropy and Clausius-Clapeyron relation for forward and reverse stress-induced martensitic transformations in polycrystalline NiTi thin-walled tubes. Mech Mater. 2020. https://doi.org/10.1016/j.mechmat.2020.103392.
16. Liu Y, Mahmud A, Kursawe F, Nam TH. Effect of pseudoelastic cycling on the Clausius-Clapeyron relation for stress-induced martensitic transformation in NiTi. J Alloys Compd. 2008;449:82–7. https://doi.org/10.1016/j.jallcom.2006.02.080.
17. Liu Y, Yang H. Strain dependence of the Clausius-Clapeyron relation for thermoelastic martensitic transformations in NiTi. Smart Mater Struct. 2007;16:22–7. https://doi.org/10.1088/0964-1726/16/1/S03.
18. Wang Z, Everaerts J, Salvati E, Korsunsky AM. Evolution of thermal and mechanical properties of NiTi wire as a function of ageing treatment conditions. J Alloys Compd. 2020. https://doi.org/10.1016/j.jallcom.2019.153024.
19. Grassi END, de Oliveira HMR, de Araujo CJ, de Castro WB. Effect of heat treatments on the thermomechanical behaviour of Ni-Ti superelastic mini coil spring. MATEC Web Conf. 2015. https://doi.org/10.1051/matecconf/20153303004.
20. Liu X, Wang Y, Yang D, Qi M. The effect of ageing treatment on shape-setting and superelasticity of a NiTi stent. Mater Charact. 2008;59:402–6. https://doi.org/10.1016/j.matchar.2007.02.007.
21. Assawakawintip T, Santiwong P, Khantachawana A, Sipiyaruk K, Chintavalakorn R. The effects of temperature and time of heat treatment on thermo-mechanical properties of custom-made NiTi orthodontic closed coil springs. Materials. 2022;15(9):31–21. https://doi.org/10.3390/ma15093121.
22. Li P, Wang Y, Meng F, Cao L, He Z. Effect of heat treatment temperature on martensitic transformation and superelasticity of the Ti49Ni51 Shape memory alloy. Materials. 2019;12:25–39. https://doi.org/10.3390/ma12162539.
23. Oncel L, Acma ME. Effect of heat treatment temperature and heat treatment time on properties and use of NiTi shape memory implant material. Int Adv Res J Sci Eng Technol. 2017;4(1):64–9. https://doi.org/10.17148/IARJSET.2017.4115.
24. Zhan C, Zee RH, Thoma PE. Effects of hafnium, heat treatment and cycling under an applied stress on the transformations of cold worked niti-based shape memory alloys. MRS Online Proc Libr. 1997;481:237–42. https://doi.org/10.1557/PROC-481-237.
25. Stoeckel D, Pelton A, Duerig T. Self-expanding NiTi stents: material and design considerations. Eur Radiol. 2004;14:292–301. https://doi.org/10.1007/s00330-003-2022-5.
26. Parente Noya, M. Self-expandable pediatric stent. ES 2914516A1 (2022).
27. Azaouzi M, Lebaal N, Makradi A, Belouettar S. Optimization based simulation of self-expanding NiTi stent. Mater Des. 2013;50:917–28. https://doi.org/10.1016/j.matdes.2013.03.012.
28. Nespoli A, Dallolio V, Villa E, Passaretti F. A new design of a NiTi ring-like wire for suturing in deep surgical field. Mater Sci Eng. 2015;56:30–6. https://doi.org/10.1016/j.msec.2015.06.009.
29. Boyle W, Cornish WE, Purtzer RA. Nichel-Titanium core guide wire. US8500658B2 (2010).
30. Petrini L, Migliavacca F. Biomedical applications of shape memory alloys. J Metallurgy. 2011. https://doi.org/10.1155/2011/501483.
31. Duerig T, Pelton A, Stockel D. An overview of NiTi medical applications. Mater Sci Eng. 1999;273–275:149–60. https://doi.org/10.1016/S0921-5093(99)00294-4.
32. Stoeckel D. NiTi medical devices and implants. MITAT. 2000; 9:81-88. https://doi.org/10.3109/13645700009063054
33. ASTM Standard F2063–18. Standard Specification for Wrought Nickel-Titanium Shape Memory Alloys for Medical Devices and Surgical Implants. ASTM International, West Conshohocken, PA 2018, https://doi.org/10.1520/F2063-18
34. Pelton AR, Russell SM, DiCello J. The physical metallurgy of nitinol for medical applications. JOM. 2003;55:33–7. https://doi.org/10.1007/s11837-003-0243-3.
35. Gall K, Tyber J, Wilkesanders G, Robertson SW, Ritchie RO, Maier HJ. Effect of microstructure on the fatigue of hot-rolled

and cold-drawn NiTi shape memory alloys. Mater Sci Eng. 2008;486:389–403. https://doi.org/10.1016/j.msea.2007.11.033.
36. Nespoli A, Villa E, Bergo L, Rizzacasa A, Passaretti F. DSC and three-point bending test for the study of the thermo-mechanical history of NiTi and NiTi-based orthodontic archwires. J Therm Anal Calorim. 2015;120:1129–38. https://doi.org/10.1007/s10973-015-4441-3.
37. Frenzel J, George EP, Dlouhy C, Somsen A, Wagner MFX, Eggeler G. Influence of Ni on martensitic phase transformations in NiTi shape memory alloys. Acta Mater. 2010;58:3444–58. https://doi.org/10.1016/j.actamat.2010.02.019.
38. Jiang SY, Zhang YG, Zhao YN, Liu SW, Hu L, Zhao GZ. Influence of Ni4Ti3 precipitates on phase transformation of NiTi shape memory alloy. Trans Nonferrous Met Soc China. 2015;25:4063–71. https://doi.org/10.1016/S1003-6326(15)64056-0.
39. Fraj B, Gahbiche A, Zghal S, Tourki Z. On the influence of the heat treatment temperature on the superelastic compressive behavior of the Ni-Rich NiTi shape memory alloy. J Mater Eng Perform. 2017;26:5660–8. https://doi.org/10.1007/s11665-017-2974-2.
40. Fan QC, Zhang YH, Wang YY, Sun MY, Meng YT, Huang SK, Wen YH. Influences of transformation behavior and precipitates on the deformation behavior of Ni-rich NiTi alloys. MSEA. 2017;700:269–80. https://doi.org/10.1016/j.msea.2017.05.107.
41. Pelton A, Dicello J, Miyazaki S. Optimization of processing of medical grade Nitinol wire. MITAT. 2009;9:107–18. https://doi.org/10.3109/13645700009063057.
42. Liu X, Wang Y, Yang D, Qi M. The effect of ageing treatment on shape-setting and superelasticity of a nitinol stent. Mater Charact. 2008;59:402–6. https://doi.org/10.1016/j.matchar.2007.02.007.
43. Lang P, Wojcik T, Povoden-Karadeniz E, Cirstea CD, Kozeschnik E. Crystal structure and free energy of Ti2Ni3 precipitates in Ti–Ni alloys from first principles. Comput Mater Sci. 2014;93:46–9. https://doi.org/10.1016/j.commatsci.2014.06.019.
44. Yahata Y, Yoneyama T, Hayashi Y, Ebihara A, Doi H, Hanawa T, Suda H. Effect of heat treatment on transformation temperatures and bending properties of nickel-titanium endodontic instruments. Int Endod J. 2009;42(7):621–6. https://doi.org/10.1111/j.1365-2591.2009.01563.x.
45. Otsuka K, Ren X. Physical metallurgy of Ti–Ni-based shape memory alloys. Prog Mater Sci. 2005;50(5):511–678. https://doi.org/10.1016/j.pmatsci.2004.10.001.
46. Huang X, Liu Y. Effect of annealing on the transformation behavior and superelasticity of NiTi shape memory alloy. Scripta Mater. 2001;45(2):153–60. https://doi.org/10.1016/S1359-6462(01)01005-3.
47. Akin E. Effect of Aging Heat Treatments on Ni52Ti48 Shape Memory Alloy. Master's thesis, Texas A&M University. 2010. https://hdl.handle.net/1969.1/ETD-TAMU-2010-08-8349
48. Arunkumar S, Kumaravel P, Velmurugan C, Senthilkumar V. Effects of thermal aging on phase transformation and microstructural characteristics of NiTi shape memory alloy. MRX. 2019;6(10):2053–1591. https://doi.org/10.1088/2053-1591/ab3b96.
49. Duerig TW, Pelton AR, Bhattacharya K. The measurement and interpretation of transformation temperatures in nitinol. Shap Mem Superelasticity. 2017;3:485–98. https://doi.org/10.1007/s40830-017-0133-0.
50. ASTM Standard F2516-07. Standard test method for tension testing of nickel-titanium superelastic materials. ASTM International, West Conshohocken, PA 2008, https://doi.org/10.1520/F2516-22
51. Liu Y. Thermodynamics of the shape memory effect in Ti–Ni alloys. In: Yoneyama T, Miyazaki S, editors. Woodhead publishing series in biomaterials, shape memory alloys for biomedical applications. Sawston: Woodhead Publishing; 2009. p. 37–68.
52. Stachowiak GB, McCormick PG. Shape memory behaviour associated with the R and martensitic transformations in a NiTi alloy. Acta Metall. 1988;36(2):291–7. https://doi.org/10.1016/0001-6160(88)90006-5.